J Biomol NMR (2011) 49:69–74
DOI 10.1007/s10858-010-9465-1

ARTICLE

Pseudo-4D triple resonance experiments to resolve HN overlap in the backbone assignment of unfolded proteins

Ireena Bagai · Stephen W. Ragsdale · Erik R. P. Zuiderweg

Received: 3 September 2010 / Accepted: 30 November 2010 / Published online: 30 December 2010

Abstract The solution NMR resonance assignment of the protein backbone is most commonly carried out using triple resonance experiments that involve ^{15}N and ^{1}HN resonances. The assignment becomes problematic when there is resonance overlap of ^{15}N–^{1}HN cross peaks. For such residues, one cannot unambiguously link the "left" side of the NH root to the "right" side, and the residues associated with such overlapping HN resonances remain often unassigned. Here we present a solution to this problem: a hybrid (4d,3d) reduced-dimensionality HN(CO)CA(CON)CA sequence. In this experiment, the Ca(i) resonance is modulated with the frequency of the Ca($i-1$) resonance, which helps in resolving the ambiguity involved in connecting the Ca(i) and Ca($i-1$) resonances for overlapping NH roots. The experiment has limited sensitivity, and is only suited for small or unfolded proteins. In a companion experiment, (4d,3d) reduced-dimensionality HNCO(N)CA, the Ca(i) resonance is modulated with the frequency of the CO($i-1$) resonance, hence resolving the ambiguity existent in pairing up the Ca(i) and CO($i-1$) resonances for overlapping NH roots.

Keywords Assignment · Unfolded proteins · Triple resonance · Reduced-dimensionality

The resonance assignment of the protein backbone is most commonly carried out using solution triple resonance experiments that involve ^{15}N and ^{1}HN resonances (Cavanagh et al. 2007). The assignment becomes problematic when these are resonance overlap of ^{15}N–^{1}HN cross peaks. Overlap occurs often in the spectra of unfolded proteins and in the spectra of flexible parts of larger proteins. If two ^{15}N–^{1}HN cross peaks overlap, it is impossible to deduce which of the two H(i)N(i)Ca(i) cross peaks in the HNCA experiment belong to which of the two H(i)N(i)Ca($i-1$) cross peaks in the HN(CO)CA experiment. Similarly, is impossible to deduce which H(i)N(i)CO($i-1$) in HNCO and/or which H(i)N(i)CB($i-1$) in HN(CO)CACB belongs to those H(i)N(i)Ca(i) cross peaks, or, for that matter, belongs to which of the H(i)N(i)CO(i) and H(i)N(i)CB(i) peaks.

In the terminology of automatic assignments (Moseley et al. 2001; Crippen et al. 2010), for such residues that have overlapping HN resonances, one cannot link the "left" side of the Generalized Spin system (GS) to the "right" side. Therefore these residues become assigned only if they are the only ones left over after everything else is assigned, or, more commonly, remain unassigned.

Here we present a strategy to assign these overlapping HN resonances using a novel hybrid (4d,3d) reduced-dimensionality (Szyperski et al. 1993; Simorre et al. 1994) **HN**(CO)CA(CON)**CA** pulse sequence, where the bold resonances are sampled conventionally, while the underlined resonance is sampled in pseudo 4D mode together with the bold CA. In the experiment, the coherence residing on ^{15}N(i) first goes to Ca($i-1$), then to Ca(i), before returning to N(i) and H(i). In this manner, one can modulate the

Electronic supplementary material The online version of this article (doi:10.1007/s10858-010-9465-1) contains supplementary material, which is available to authorized users.

I. Bagai · S. W. Ragsdale
Department of Biological Chemistry, University of Michigan Medical School, MSRB III, 1150 W. Medical Center Drive, Ann Arbor, MI 48109-5605, USA

E. R. P. Zuiderweg (✉)
Department of Biological Chemistry, University of Michigan Medical School, 4220D MSRB III, 1150 W. Medical Center Drive, Ann Arbor, MI 48109-5605, USA
e-mail: zuiderwe@umich.edu

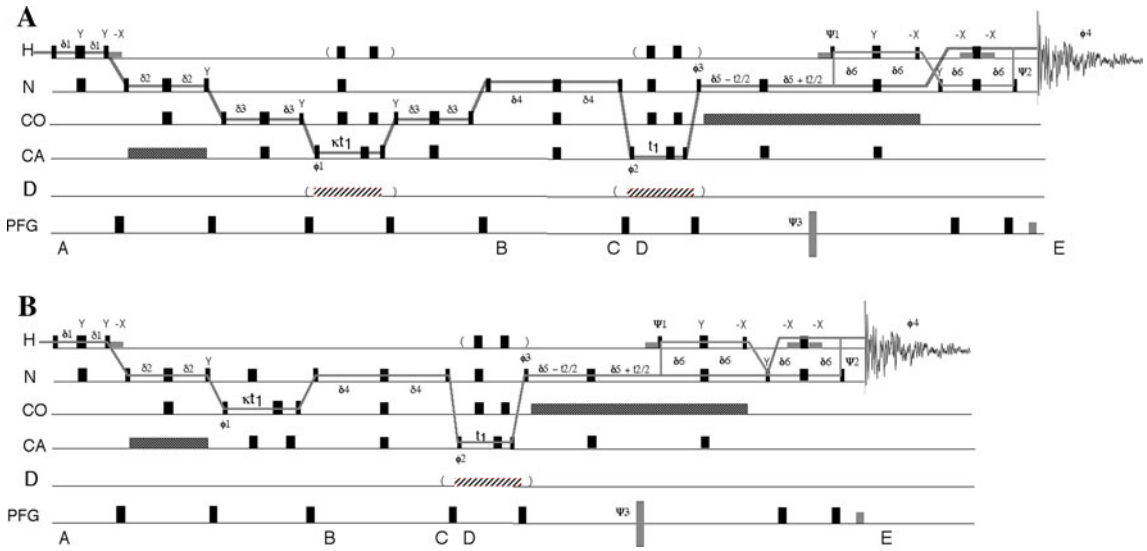

Fig. 1 **a** The (4d,3d) **HN**(CO)CA(CON)**CA** sequence. **b** The (4d,3d) **HN**CO(N)**CA** sequence. The sequences are HNCOCA (Fig. 1a) or HNCO (Fig. 1b) from point A to B. From B to C is a transfer, and from D to E, the sequences are HNCA-TROSY, in an implementation combining publications of different groups (Rance et al. 1999; Schulte-Herbruggen and Sorensen 2000; Loria et al. 1999; Salzmann et al. 1998). 90° pulses are narrow boxes, 180° pulses are wide boxes. The 180° CO/Ca pulses are selective by using a 41 μs pulse length (800 MHz). The gray pulses are selective for the H_2O resonance (≈800 ms). The ^{1}H 180° pulses in parentheses can be omitted if the protein is (perfectly) perdeuterated. The gray gradient pulses achieve ^{15}N–^{1}H echo-anti-echo coherence selection. All pulses have x-phase, unless noted differently. $\psi 1 = -y$, $\psi 2 = -x$, $\psi 3 =$ negative. Phase cycle: $\phi 1 =$ x, −x; $\phi 2 =$ x, x, −x, −x; $\phi 3 =$ y, $\phi 4 = +, -, -, +$. States-tppi quadrature in t_1 is achieved by incrementing $\phi 2$ by 90° in odd t_1-counts and both $\phi 2$ and $\phi 4$ with 180° in even t_1-counts. Sensitivity-enhanced single-transition-to-single-transition echo-anti echo tppi in t_2 is achieved by incrementing $\psi 1$, $\psi 2$ by 180° and the sign of the gradient $\psi 3$ in odd t_2 counts, and $\phi 3$ and $\phi 4$ with 180° in even t_2 counts. The delays are: $\delta 1$: optimum for $\sin(2\pi J^{HN}\ \delta 1)\exp(-2\delta 1/T_{2H}) \approx 2.4$ ms. $\delta 2$: optimum for $\sin(2\pi J^{NC'}\ \delta 2)\exp(-2\delta 2/T_{2N}) \approx 11$ ms. $\delta 3$: optimum for $\sin(2\pi J^{C'Ca}\delta 3)\exp(-2\delta 3/T_{2C'}) \approx 4.5$ ms. $\delta 4$: optimum for $\sin(2\pi J^{NC'}\delta 4)\ \sin(2\pi J^{NCai}\delta 4)\ \cos(2\pi J^{NCa(i-1)}\delta 4)\exp(-2\delta 4/T_{2N}) \approx 13$ ms. $\delta 5{+}\delta 6$: optimum for $\sin(2\pi J^{NCai}(\delta 5{+}\delta 6))\ \cos(2\pi J^{NCa(i-1)}(\delta 5{+}\delta 6))\exp(-2(\delta 5{+}\delta 6)/T_{2N} \approx 12$ ms. $\delta 6$: $1/4J_{NH} = 2.75$ ms. The pseudo 4D incrementation can be scaled with κ; we used $\kappa = 1$. Cosine modulation is obtained with the given phase $\phi 1$; sine modulation is obtained by using $\phi 1 =$ y, −y and applying a zero-order 90° phase correction in the ^{13}C dimension during data processing

Ca(i) resonance with the frequency of the Ca($i-1$) resonance, hence resolving the ambiguity associated with connecting the Ca(i) and Ca($i-1$) resonances in GSs of the overlapping resonances. We also present a companion experiment, a hybrid (4d,3d) reduced-dimensionality **HN**CO(N)**CA** sequence, resolving the ambiguity associated with connecting the Ca(i) and CO($i-1$) resonances in GSs of the overlapping resonances.

Figure 1 shows the pulse sequences of the **HN**(CO)CA(CON)**CA** and **HN**CO(N)**CA**. The sequences are HNCOCA (Fig. 1a) or HNCO (Fig. 1b) from point A to B.

For both experiments, the density operator at point B is given as:

$$\rho(B) \propto 4H_Z C'_Z N_y \cos\left(\Omega^{C\alpha i-1}\kappa t_1\right).$$

Between B and C, $J^{NC'}$, $J^{NC\alpha i}$ and $J^{NC\alpha i-1}$ are active, hence causing the density operator to evolve as:

The transfer functions for these terms are plotted in Fig. 2.

Both $4H_Z C^{\alpha}_Z N_y$ terms are converted to $4H_Z C^{\alpha}_y N_z$ at point D, after which a standard HNCA-TROSY or HNCA-HSQC sequence is executed. The Ca($i-1$) frequency of the HNCOCA part is jointly sampled with the Ca frequencies of the HNCA part in a pseudo-4d (GFT) manner (Shen et al. 2005; Atreya and Szyperski 2004). The given phase program $\varphi 1$ in Fig. 1 yields a cosine modulation of the t_1 period, giving rise to in-phase doublets with splittings corresponding to twice the frequency difference of the Ca($i-1$) resonance with the ^{13}C carrier (for $\kappa = 1$). A separate experiment is collected with phase $\varphi 1$ incremented by 90°, giving rise to an anti-phase doublet. Addition or subtraction of the sine and cosine experiments results in an HNCA-like spectrum, in which both Ca(i) and Ca($i-1$) resonances are shifted by the signed difference

$$\rho(C) \propto \cos\left(\Omega^{C\alpha i-1}\kappa t_1\right)\left\{\begin{array}{r} 4H_Z C^{\alpha i}_Z N_y \sin\left(\pi J^{NC'}\tau\right)\sin\left(\pi J^{NC\alpha i}\tau\right)\cos\left(\pi J^{NC\alpha i-1}\tau\right) \\ +4H_Z C^{\alpha i-1}_Z N_y \sin\left(\pi J^{NC'}\tau\right)\cos\left(\pi J^{NC\alpha i}\tau\right)\sin\left(\pi J^{NC\alpha i-1}\tau\right) + \text{other terms} \end{array}\right\}.$$

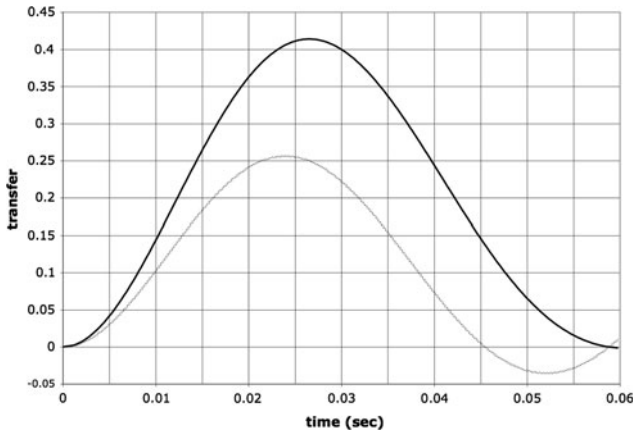

Fig. 2 Transfer efficiencies for $\sin(\pi J^{NC'} t)\ \sin(\pi J^{NCai} t)\ \cos(\pi J^{NCa(i-1)} t)\exp(-R_{2N} t)$ (for Ca(i) cross peaks in HNCA; solid) and $\sin(\pi J^{NC'} t)\ \cos(\pi J^{NCai} t)\ \sin(\pi J^{NCa(i-1)} t)\exp(-R_{2N} t)$ (for Ca($i-1$) cross peaks in HNCA; dashed) with $J^{NC'} = 17$ Hz, $J^{NCai} = 11$ Hz, $J^{NCa(i-1)} = 8$ Hz and $R_{2N} = 15\ s^{-1}$

frequency of the Ca($i-1$) resonance with the ^{13}C carrier position.

The **HN**(CO)CA(CON)**CA** sequence was used to complete the assignments for the 79-residue unfolded C-terminal region of human heme oxygenase-2 (Yi et al. 2009). Figure 3a shows the results for several non-degenerate examples. Here we have overlaid the HNCA, HN(CO)CA and the sum of the cosine- and sine-modulated **HN**(CO)CA(CON)**CA** experiments. As illustrated with the colored brackets, the HNCA peaks are shifted by the signed difference frequency of the HN(CO)CA peak with the ^{13}C carrier. As mentioned, both Ca(i) and Ca($i-1$) cross peaks are shifted in the pseudo 4D experiment; however, the shifted Ca($i-1$) peak is in most cases too small to be observed. The dashed bracket in Fig. 3a points to a shifted Ca($i-1$) peak that did come through. Figure 3b shows the results for the resonances D29 and L68 of the protein for which the NH

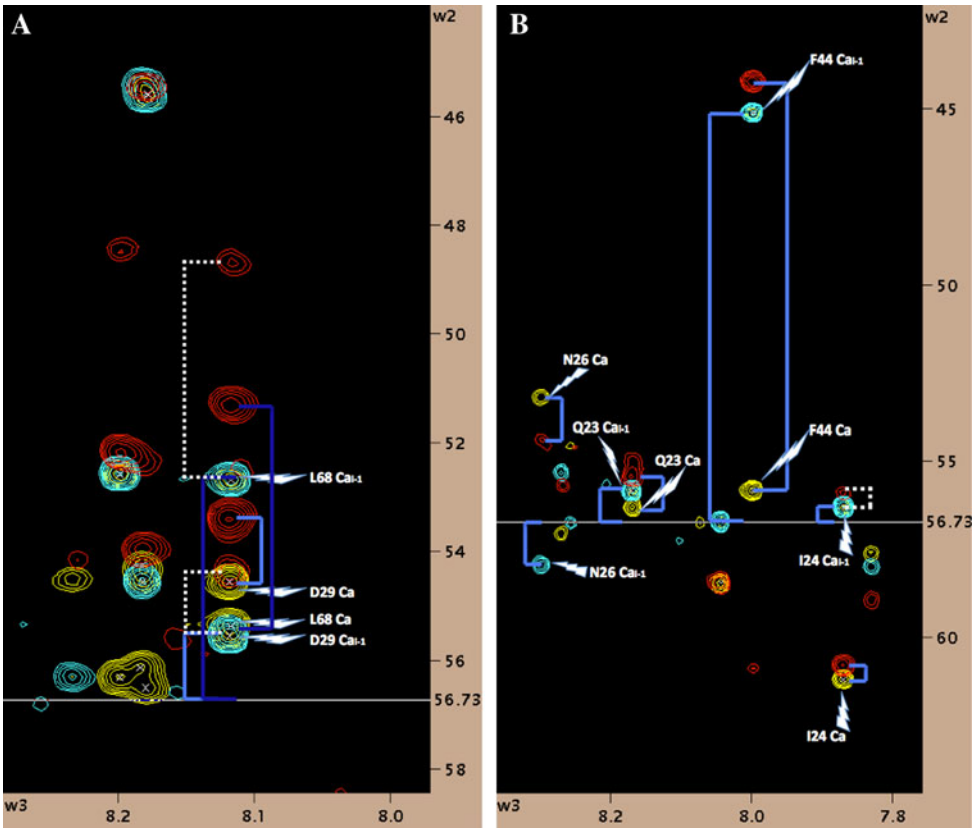

Fig. 3 Overlays of standard 3d-HNCA-TROSY (*yellow*), standard 3d-HN(CO)CA-TROSY (*cyan*) and the sum of the cosine and sine modulated (4d,3d) **HN**(CO)CA(CON)**CA** experiments (*red*). The horizontal line at 56.73 ppm indicates the position of the ^{13}C carrier. **a** *Blue "left-hand" brackets* identify the Ca($i-1$)—carrier difference frequencies in the HNCOCA; the *"right-handed" brackets* show how the Ca(i) in the pseudo 4D are shifted by these difference frequencies. The dashed bracket shows a shifted Ca($i-1$) peak. Resonance assignments obtained by SAGA (Crippen et al. 2010) are indicated. **b** *Light and dark blue brackets* show the pairing of Ca(i) and Ca($i-1$) for two different spins systems, for which the NH frequencies are completely degenerate. The 79-residue disordered C-terminal region of human heme oxygenase-2 (HO2) was ^{13}C,^{15}N labeled. Sample conditions: 1 mM HO2, 50 mM Tris, 100 mM KCl, pH 7.0, 18°C. The data was acquired on an Oxford 800 MHz magnet equipped with a Varian NMR SYSTEM console and a room temperature triple resonance gradient probe. The HNCA-TROSY, HN(CO)CA-TROSY, (4d,3d) **HN**(CO)CA(CON)**CA** cosine and (4d,3d) **HN**(CO)CA(CON)**CA** sine experiments were collected with 75 and 45 complex points in t_1 and t_2, respectively, and with 2 transients per increment in 9.5 h each

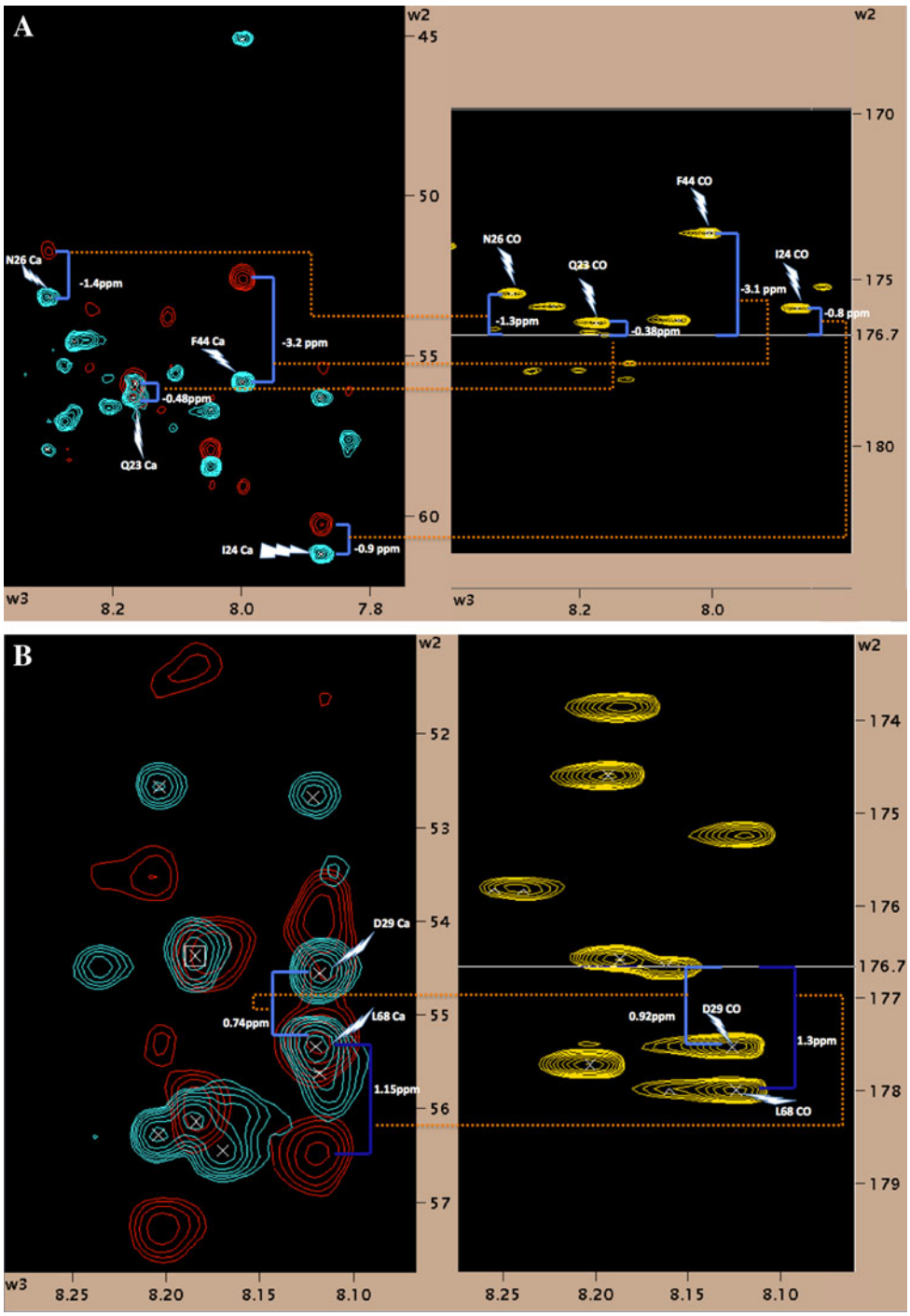

Fig. 4 Overlays of standard 3d-HNCA-TROSY (*cyan*) and the sum of the cosine and sine modulated (4d,3d) **HN**CO(N)**CA** spectra (*red*), at *left*. The standard 3D-HNCO-TROSY experiment, at *right*. The horizontal line at 176.7 ppm indicates the position of the ^{13}C carrier. The (4d,3d) **HN**CO(N)**CA** cosine and (4d,3d) **HN**CO(N)**CA** sine experiments were collected with 80 and 30 complex points in t_1 and t_2, respectively, and with 4 transients per increment in 9.0 h each. Sample conditions were same as stated in Fig. 3. **a** *Blue brackets* in the right panel identify the CO($i-1$)—carrier difference frequencies in the HNCO; brackets in the left panel show how Ca(i) in the pseudo 4D are shifted by these difference frequencies. *Dashed orange connectors* are used to point at the corresponding modulations in the HNCO and HNCA respectively. Resonance assignments obtained by SAGA (Crippen et al. 2010) are indicated. **b** *Light and dark blue brackets* show the pairing of CO($i-1$) and Ca(i) for two different spins systems, for which the NH frequencies are completely degenerate. The slight discrepancy in the chemical shift differences between the left and right spectra is accounted for by the fact that the HNCO used here for comparison, was run earlier using a sample from a different preparation of HO2

cross-peaks have identical frequencies, resulting in two HN(CO)CA peaks that have the H and N coordinates in common. The analysis shows how the ambiguity of Ca(i) with Ca($i-1$) pairing is solved (dark blue: pairing for L68; light blue: pairing for D29). Several shifted Ca($i-1$) peaks are also showing, as indicated with the dashed brackets. For our project, this sufficed to obtain the connectivity and assignments for the overlapping HN peaks.

Although not used for initial assignments, the **HN**CO(N)**CA** experiment was performed to confirm the connectivity between CO($i-1$) and Ca(i) of residues with degenerate HN shifts. Figure 4a shows the results for the same non-degenerate examples as depicted in Fig. 3a. The left panel of the figure is an overlay of HNCA and the sum of the cosine- and sine-modulated **HN**CO(N)**CA** spectra, whereas the right panel shows an HNCO spectrum

synchronized in the H and N dimensions with respect to HNCA. Again, as illustrated with the colored brackets, the HNCA peaks are shifted by the (signed) difference frequency of the HNCO peak with the ^{13}C carrier. Figure 4b shows results for resonances D29 and L68 that have identical NH cross-peak frequencies and therefore the two corresponding Ca(i) peaks fall on the same N, H coordinates. The analysis, again shows how the ambiguity of Ca(i) with CO($i-1$) pairing is solved (dark blue: pairing for L68; light blue: pairing for D29).

The sensitivity of the **HN**(CO)CA(CON)**CA** and **HN**CO(N)**CA** experiments is limited, since the extra transfer reduces S/N by 60% as compared to the HN(CO)CA or HNCO (see Fig. 2). The pseudo-4D cosine or sine modulations generate doublets, which when co-added further reduce sensitivity by a factor of $\sqrt{2}$. Finally, the Ca(i) linewidth in **HN**(CO)CA(CON)**CA** is increased by κ*(Ca($i-1$)) linewidth, which is approximately a factor of 2 when $\kappa = 1$, assuming the Ca(i) and Ca($i-1$) line widths are about the same. In total, the **HN**(CO)CA(CON)**CA** sensitivity is reduced by a factor of about 5 as compared to an HNCOCA. The **HN**CO(N)**CA** sensitivity as compared to HNCO contains the same factors, but the effect of the pseudo-4D sampling of the composite CO ($i-1$)-Ca(i) linewidth as compared to the CO($i-1$) are more severe and also depends, because of the CO-CSA relaxation, on B_0. We estimate that the total sensitivity of **HN**CO(N)**CA** as compared to HNCO is down by a factor of 10. Hence the use of both experiments is restricted to unfolded proteins or unfolded protein areas with high intrinsic S/N. The TROSY version of the experiments may also be used for the folded areas of highly soluble larger proteins, if one is willing to invest a week of instrument time. Likely, the sensitivity of HNCA-SE-HSQC versions of the experiments (not shown) would be better for unfolded proteins when lower-field spectrometers are used.

The **HN**(CO)CA(CON)**CA** experiment could also be set-up as a (5d,3d) **HN**COCA(CON)**CA** in which the CO($i-1$) is co-sampled with the Ca(i) or N(i). This would unambiguously identify which CO ($i-1$) belongs to which Ca(i), which will also be of help in continuing assignments over two or more degenerate NH's. However, this additional (constant-time) evolution will cause further decrease in sensitivity. Better is to use the more sensitive (4d,3d) **HN**CO(N)**CA** experiment to identify which CO($i-1$) belongs to which Ca(i) (see Fig. 1b and 4). Extension of this approach can be visualized, e.g., a (4d,3d) **HN**CO(N)**CACB** would identify which CO($i-1$) belongs to which Cb(i). Obviously, the experiment's low sensitivity would severely limit its application.

Finally, the (4d,3d) **HN**(CO)CA(CON)**CA** and **HN**CO(N)**CA** experiments may be recorded with different values for κ, after which projection reconstructions methods could be applied to regenerate the full 4D spectrum (Kupce and Freeman 2004, 2006; Hiller et al. 2005). Whether such additional experiments and processing would be helpful for data interpretation depends on the severity of overlap in the NH spectrum.

Once the proper Ca(i) with Ca($i-1$) and CO($i-1$) pairings are accomplished, the remaining ambiguities can be solved with other (reduced dimensionality) experiments. For example, (4d,3d) GFT HNCOCA (Atreya and Szyperski 2004) or APSY6D HNCOCAHN (Fiorito et al. 2006) allows for the correct pairing of CO($i-1$) with Ca ($i-1$)s; (4d,3d) GFT HNCACO (Atreya and Szyperski 2004) may be used to pair up CO(i)s with corresponding Ca(i)s. Similarly, (4d,3d) GFT HNCACB-CA (Atreya and Szyperski 2004) could provide for the correct pairing of Ca(i)s with Cb(i)s and possibly Ca($i-1$)s with Cb($i-1$)s, while APSY7D HNCOCACBHN (Hiller et al. 2007) will pair Ca($i-1$) with Cb($i-1$)'s.

Acknowledgments We acknowledge NIH R01HL 102662; ERPZ also acknowledges NIH ARRA GM063027-S2.

References

Atreya HS, Szyperski T (2004) G-matrix Fourier transform NMR spectroscopy for complete protein resonance assignment. Proc Natl Acad Sci U S A 101(26):9642–9647

Cavanagh J, Fairbrother W, Palmer AG III, Rance M, Skelton NJ (2007) Protein NMR spectroscopy: principles and practice, 2nd edn. Elsevier Academic Press, Amsterdam

Crippen GM, Rousaki A, Revington M, Zhang Y, Zuiderweg ER (2010) Saga: rapid automatic mainchain NMR assignment for large proteins. J Biomol NMR 46(4):281–298

Fiorito F, Hiller S, Wider G, Wuthrich K (2006) Automated resonance assignment of proteins: 6d apsy-NMR. J Biomol NMR 35(1):27–37

Hiller S, Fiorito F, Wuthrich K, Wider G (2005) Automated projection spectroscopy (apsy). Proc Natl Acad Sci USA 102(31):10876–10881

Hiller S, Wasmer C, Wider G, Wuthrich K (2007) Sequence-specific resonance assignment of soluble nonglobular proteins by 7d apsy-NMR spectroscopy. J Am Chem Soc 129(35):10823–10828

Kupce E, Freeman R (2004) Projection-reconstruction technique for speeding up multidimensional NMR spectroscopy. J Am Chem Soc 126(20):6429–6440

Kupce E, Freeman R (2006) Hyperdimensional NMR spectroscopy. J Am Chem Soc 128(18):6020–6021

Loria JP, Rance M, Palmer AG III (1999) Transverse-relaxation-optimized (trosy) gradient-enhanced triple-resonance NMR spectroscopy. J Magn Reson 141(1):180–184

Moseley HN, Monleon D, Montelione GT (2001) Automatic determination of protein backbone resonance assignments from triple resonance nuclear magnetic resonance data. Methods Enzymol 339:91–108

Rance M, Loria JP, AGr Palmer (1999) Sensitivity improvement of transverse relaxation-optimized spectroscopy. J Magn Reson 136(1):92–101

Salzmann M, Pervushin K, Wider G, Senn H, Wuthrich K (1998) Trosy in triple-resonance experiments: new perspectives for sequential NMR assignment of large proteins. Proc Natl Acad Sci U S A 95(23):13585–13590

Schulte-Herbruggen T, Sorensen OW (2000) Clean trosy: compensation for relaxation-induced artifacts. J Magn Reson 144(1): 123–128

Shen Y, Atreya HS, Liu G, Szyperski T (2005) G-matrix fourier transform noesy-based protocol for high-quality protein structure determination. J Am Chem Soc 127(25):9085–9099

Simorre JP, Brutscher B, Caffrey MS, Marion D (1994) Assignment of NMR spectra of proteins using triple-resonance two-dimensional experiments. J Biomol NMR 4(3):325–333

Szyperski T, Wider G, Bushweller J, Wuthrich K (1993) Reduced dimensionality in triple-resonance NMR experiments. J Am Chem Soc 115:9307–9308

Yi L, Jenkins PM, Leichert LI, Jakob U, Martens JR, Ragsdale SW (2009) Heme regulatory motifs in heme oxygenase-2 form a thiol/disulfide redox switch that responds to the cellular redox state. J Biol Chem 284(31):20556–20561